

The branching ratio $\omega \rightarrow \pi^+ \pi^-$ revisited

C. Hanhart¹, S. Holz², B. Kubis^{2,3,a}, A. Kupść^{4,5}, A. Wirzba^{1,6}, C. W. Xiao¹

¹Institut für Kernphysik, Institute for Advanced Simulation, and Jülich Center for Hadron Physics, Forschungszentrum Jülich, 52425 Jülich, Germany

²Helmholtz-Institut für Strahlen- und Kernphysik, Universität Bonn, 53115 Bonn, Germany

³Bethe Center for Theoretical Physics, Universität Bonn, 53115 Bonn, Germany

⁴Division of Nuclear Physics, Department of Physics and Astronomy, Uppsala University, Box 516, 75120 Uppsala, Sweden

⁵High Energy Physics Department, National Centre for Nuclear Research, ul. Hoza 69, 00-681 Warsaw, Poland

⁶Kavli Institute for Theoretical Physics, Kohn Hall, University of California, Santa Barbara, CA 93106-4030, USA

Abstract We analyze the most recent data for the pion vector form factor in the timelike region, employing a model-independent approach based on dispersion theory. We confirm earlier observations about the inconsistency of different modern high-precision data sets. Excluding the BaBar data, we find an updated value for the isospin-violating branching ratio $\mathcal{B}(\omega \rightarrow \pi^+ \pi^-) = (1.46 \pm 0.08) \times 10^{-2}$. As a side result, we also extract an improved value for the pion vector or charge radius, $\sqrt{\langle r_V^2 \rangle} = (0.6603 \pm 0.0005) \text{ fm}$. In addition, we demonstrate that modern high-quality data for the decay $\eta' \rightarrow \pi^+ \pi^- \gamma$ will allow for an even improved determination of the transition strength $\omega \rightarrow \pi^+ \pi^-$.

Keywords Dispersion relations · Meson–meson interactions · Chiral symmetries

PACS 11.55.Fv · 13.75.Lb · 11.30.Rd

1 Introduction

In recent years interest in high-quality pion form factor data below $s = 1 \text{ GeV}^2$ has increased tremendously, since it provides a crucial input to quantify the Standard Model prediction for the hadronic contribution to the muon anomalous magnetic moment (see, e.g., Refs. [1, 2, 3] and references therein) and the dispersion integral that needs be evaluated in this context puts a lot of weight on the low-energy transition $\gamma^* \rightarrow \text{hadrons}$. To make the most of the existing data, it is compulsory to employ model-independent theoretical tools that allow for an appropriate parametrization of the data, but also for a judgment on their consistency. For the two-pion contributions to the above-mentioned transitions the appropriate tool is again dispersion theory, for it allows one to use the high-quality information available for pion–pion scattering [4, 5, 6, 7] in the form factor analysis in a way

consistent with analyticity and unitarity. The strong impact these theoretical constraints can have on our understanding of the pion form factor has been emphasized and used to good effect several times before [8, 9, 10, 11, 12, 13, 14], with some of those references very close in spirit to what we are attempting here.

We exemplify the power of this formalism by an analysis of the most recent data sets for the pion vector form factor extracted from measurements of $e^+ e^- \rightarrow \pi^+ \pi^-$, with the specific goal to extract an update on the partial width for $\omega \rightarrow \pi^+ \pi^-$. As a side result we also determine an updated value for the pion vector or charge radius. Since final-state interactions are universal within the same scheme, we also propose to analyze the reaction $\eta' \rightarrow \pi^+ \pi^- \gamma$: not only will high-quality data for this reaction become available from different experiments in the very near future, but also it is shown to provide additional, independent access to the $\omega \rightarrow \pi^+ \pi^-$ transition strength. To illustrate the potential accuracy of such a determination once the new data are available, we here analyze pseudo-data generated according to preliminary results from BESIII [15].

One key feature of the formalism employed here is that it makes maximal use of the universal phase introduced by the pion–pion final-state interactions. In particular, we do not have the freedom to add Breit–Wigner functions with arbitrary relative phases. This allows us to extract the relevant amplitudes in a controlled fashion. As a side note, we illustrate the reaction-dependence of Breit–Wigner functions explicitly by demonstrating that a (constant) complex phase in the coupling and a shift of the ω mass parameter lead to similar effects on the observables.

This paper is organized as follows. In Sect. 2, we lay out the necessary formalism, introducing the dispersive representations of both the pion vector form factor and the $\eta' \rightarrow \pi^+ \pi^- \gamma$ decay amplitude and showing how the parameters of the ρ – ω mixing signals can be related to the decay width

^ae-mail: kubis@hiskp.uni-bonn.de

of $\omega \rightarrow \pi^+\pi^-$. This is followed in Sect. 3 by a detailed discussion of the results for the $\omega \rightarrow \pi^+\pi^-$ branching fraction, obtained from elaborate fits both to various $e^+e^- \rightarrow \pi^+\pi^-$ data sets as well as the BESIII pseudo-data for the decay $\eta' \rightarrow \pi^+\pi^-\gamma$. Section 4 presents our findings on the pion vector radius. We close with a summary.

2 Formalism

2.1 Matrix elements

The pion vector form factor $F_V(s)$, which describes the reaction $e^+e^- \rightarrow \pi^+\pi^-$, is defined by the vector current matrix element

$$\langle \pi^+(k_+)\pi^-(k_-) | \mathcal{V}^\mu | 0 \rangle = e(k_+ - k_-)^\mu F_V(s),$$

$$s = q^2, \quad q^\mu = k_+^\mu + k_-^\mu, \quad (1)$$

where $e > 0$ is the unit of the electric charge. Throughout this work we apply the definition $\mathcal{V}^\mu = -\delta \mathcal{L}_{\text{int}} / \delta A_\mu$, with the photon field A_μ . For the pion fields, we use the Condon–Shortley sign convention $\pi^\pm = \mp(\pi^1 \mp i\pi^2)/\sqrt{2}$.

The matrix element describing the decay $\eta' \rightarrow \pi^+\pi^-\gamma$ in the P -wave approximation can be written as¹

$$\langle \pi^+(k_+)\pi^-(k_-) | \mathcal{V}_\mu | \eta'(p) \rangle = \varepsilon_{\mu\nu\alpha\beta} p^\nu k_+^\alpha k_-^\beta f_1(s) \quad (2)$$

(see Ref. [18] for a definition of the partial-wave expansion). We define $\varepsilon_{\mu\nu\alpha\beta}$ such that $\varepsilon_{0123} = +1$. The corresponding differential decay rate is given by

$$\frac{d\Gamma(\eta' \rightarrow \pi^+\pi^-\gamma)}{d\sqrt{s}} = |f_1(s)|^2 \Gamma_1(s), \quad (3)$$

where the function

$$\Gamma_1(s) = \frac{4}{3} \left(\frac{m_{\eta'}^2 - s}{16\pi m_{\eta'}} \sqrt{s - 4m_\pi^2} \right)^3 \quad (4)$$

collects the phase-space terms and kinematical factors of the modulus squared of the invariant matrix element for the point-particle case [19], with $m_{\eta'}$ and m_π denoting the mass of the η' and the pion, respectively.

2.2 Universality of final-state interactions and dispersive representations

We base our analysis on the fact that as a result of unitarity, all elastic pion–pion ($\pi\pi$) interactions of a definite partial wave are largely determined by a single, universal function given in terms of the corresponding $\pi\pi$ phase shift—the

¹We use the sign and phase assignments according to Refs. [16, 17], adapted for the fact that both works implicitly assume a negative value for e and do not follow the Condon–Shortley convention.

Omnès function $\Omega(s)$, depending only on s , the squared invariant mass of the outgoing pion pair. For pion pairs with relative angular momentum $L = 1$, it is given by

$$\Omega(s) = \exp \left\{ \frac{s}{\pi} \int_{4m_\pi^2}^{\infty} dx \frac{\delta_1(x)}{x(x-s-i\epsilon)} \right\}, \quad (5)$$

where $\delta_1(s)$ denotes the pion–pion P -wave phase shift. The Omnès function captures the physics of the ρ -meson, encoded in the phase shift in a model-independent way, thus eschewing the need to use a model like vector-meson dominance. Recent phase shift analyses based on sophisticated dispersive analyses are available from the Madrid [6] and Bern [7] groups in an energy range from threshold up to about 1.4 GeV. In our analysis, we continue these phase shifts smoothly to an asymptotic value of π above 1.3 GeV and 1.42 GeV, respectively, in order to fix $\Omega(s)$ completely. As we are interested in an evaluation of the Omnès function only for energies below 1 GeV, the precise rate at which this limiting value is approached is immaterial: it leads to changes in the Omnès function that can be absorbed in the parametrizations used in this work.

In Refs. [19, 20], the universality of the final-state interactions was used to express $F_V(s)$ and $f_1(s)$ in the forms

$$F_V(s) = R(s)\Omega(s), \quad f_1(s) = P(s)\Omega(s). \quad (6)$$

The functions $R(s)$ and $P(s)$ must be real and free of right-hand cuts in the elastic region; in Refs. [19, 20] they were assumed to be linear polynomials, which was demonstrated to be sufficient for the (isospin-related) vector form factor featuring in the decay $\tau^- \rightarrow \pi^-\pi^-\nu_\tau$, as well as the decay $\eta \rightarrow \pi^+\pi^-\gamma$ [21, 22] similar to the η' transition. The universal phase that $F_V(s)$ and $f_1(s)$ share with the Omnès function, given by $\delta_1(s)$, is a consequence of Watson’s final-state theorem [23]. The formalism for the η' decay was improved further in Ref. [18], where it was shown that $P(s)$ contains a left-hand cut induced by tensor-meson ($a_2(1320)$) exchange, which in the physical decay region can be approximated to very good precision by the inclusion of a quadratic term in $P(s)$.

However, the expressions given so far ignore the contribution from the ω -meson, which can also decay into the $\pi^+\pi^-$ final state via isospin-violating interactions. While we assume isospin symmetry everywhere else, this particular isospin-breaking effect is enhanced by a small energy denominator, as the ω -resonance is very narrow and close in mass to the ρ , the dominant resonant enhancement of the $\pi\pi$ P -wave amplitude. It is well-known that the inclusion of this mechanism, often named ρ – ω mixing, is essential for an accurate description of the vector form factor in $e^+e^- \rightarrow \pi^+\pi^-$. In this paper we extend the formalism of Refs. [18, 19, 20] to include this effect, which gives access to the $\omega \rightarrow \pi^+\pi^-$ transition strength. The contributions of the ω are shown diagrammatically in Figs. 1 and 2. In both

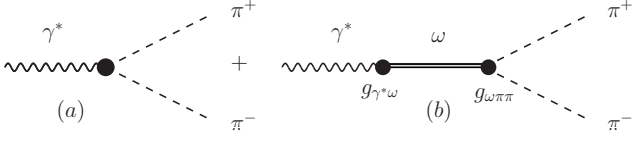


Fig. 1 Diagrammatic representation of the reaction $\gamma^* \rightarrow \pi^+ \pi^-$. The pions from both diagrams undergo final-state interactions that are not shown explicitly.

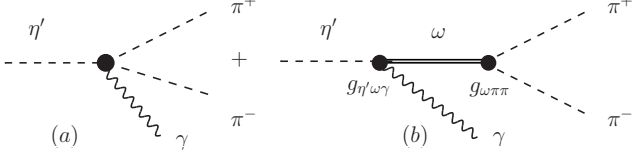


Fig. 2 Diagrams contributing to the reaction $\eta' \rightarrow \pi^+ \pi^- \gamma$. The pions from both diagrams undergo final-state interactions that are not shown explicitly.

cases the outgoing pion pair undergoes final-state interactions in the P -wave, which are universal and controlled by the Omnès function. In the ω -channel on the other hand, the use of a Breit–Wigner function appears to be justified, since the ω total width is small, $\Gamma_\omega^{\text{tot}} = (8.49 \pm 0.08) \text{ MeV}$ [24]. Our generalization of the polynomials $R(s)$ and $P(s)$ now reads

$$R(s) = 1 + \alpha_V s + \frac{\kappa_1 s}{m_\omega^2 - s - im_\omega \Gamma_\omega^{\text{tot}}}, \quad (7)$$

$$P(s) = A(1 + \alpha s + \beta s^2) + \frac{\kappa_2}{m_\omega^2 - s - im_\omega \Gamma_\omega^{\text{tot}}}, \quad (8)$$

where m_ω denotes the ω mass and α_V , α , β , κ_1 , and κ_2 are constants to be determined from a fit to data. Equations (7) and (8) are correct to leading order in isospin violation. Unitarity dictates that after the transition from the ω -meson to a pion pair, the phase induced by the final-state interaction must again be equal to that of pion–pion P -wave scattering. This leads to the requirement that both κ_1 and κ_2 are real-valued. This statement also holds up to higher orders in isospin violation, which are expected to provide negligible corrections. Similar ansätze for the ρ – ω mixing term were used before frequently [10, 12, 13, 25, 26, 27]; we employ the sign convention of Ref. [27]. Note that we checked that the inclusion of higher-order terms in the polynomials in $R(s)$ and $P(s)$ does not change the values for $\kappa_{1/2}$ extracted phenomenologically.

2.3 The relation to $\Gamma(\omega \rightarrow \pi^+ \pi^-)$

The parameters $\kappa_{1/2}$ are proportional to the coupling strength of the ω to two pions $g_{\omega\pi\pi}$, see Figs. 1 and 2, which in turn can be related to the partial decay width $\omega \rightarrow \pi^+ \pi^-$. To calculate the factor of proportionality we need to utilize proper vertex functions as outlined below. This subsection is devoted to establishing the connection in such a way that

$\Gamma(\omega \rightarrow \pi^+ \pi^-)$ can be determined from an extraction of $\kappa_{1/2}$ in a fit to the available data.

In order to connect $g_{\omega\pi\pi}$ to the quantities κ_1 and κ_2 defined in Eqs. (7) and (8), we first derive the $\omega \rightarrow \pi^+ \pi^-$ vertex

$$\langle \pi^+(k_+) \pi^-(k_-) | \mathcal{L}_{\omega\pi\pi} | \omega(q) \rangle = -g_{\omega\pi\pi} \epsilon_\mu^{(\omega)}(q) (k_+ - k_-)^\mu, \quad (9)$$

with $\epsilon_\mu^{(\omega)}(q)$ the pertinent polarization vector of the vector meson ω of momentum q , from the interaction Lagrangian

$$\mathcal{L}_{\omega\pi\pi} = ig_{\omega\pi\pi} (\pi^- \partial^\mu \pi^+ - \pi^+ \partial^\mu \pi^-) \omega_\mu, \quad (10)$$

which is the analog of the $\gamma\pi\pi$ Lagrangian with $g_{\omega\pi\pi}$ and the vector field ω_μ of the ω -meson taking over the role of the charge e and the photon field A_μ , respectively; see also Ref. [17], as well as Ref. [28] for a comprehensive overview of vector-meson Lagrangians. Furthermore, we need the coupling of the ω to a virtual photon as well as the vertex for $\eta' \rightarrow \omega \gamma$. For the former we use the effective Lagrangian [17, 29]

$$\mathcal{L}_{\omega\gamma} = -\frac{e}{2} g_{\omega\gamma} F^{\mu\nu} \omega_{\mu\nu}, \quad (11)$$

where $F_{\mu\nu} = \partial_\mu A_\nu - \partial_\nu A_\mu$ is the electromagnetic field strength tensor and $\omega_{\mu\nu} = \partial_\mu \omega_\nu - \partial_\nu \omega_\mu$. Contrary to standard vector-meson dominance formulations, we couple the ω -meson (with the coupling strength $g_{\omega\gamma}$) to the electromagnetic field strength tensor and not to the vector field in order to ensure gauge invariance directly on the level of the vertex. The additional derivatives that accompany this choice are the origin of the factor $s (= q^2)$ in Eq. (7); the corresponding vertex reads

$$\langle \omega(q) | \mathcal{V}_\mu | 0 \rangle = e g_{\omega\gamma} q^2 \epsilon_\mu^{(\omega)}(q). \quad (12)$$

Furthermore, when taking $q^2 = m_\omega^2$ and neglecting the electron mass, the $e^+ e^-$ decay width of the ω is given by

$$\Gamma(\omega \rightarrow e^+ e^-) = \frac{4\pi\alpha_{\text{em}}^2}{3} g_{\omega\gamma}^2 m_\omega, \quad (13)$$

with $\alpha_{\text{em}} \approx 1/137.036$ the electromagnetic fine structure constant. Using $\Gamma(\omega \rightarrow e^+ e^-) = (0.60 \pm 0.02) \text{ keV}$ [24], we obtain

$$|g_{\omega\gamma}| = (5.9 \pm 0.1) \times 10^{-2}. \quad (14)$$

In this way one finds for the transition $\gamma^* \rightarrow \omega \rightarrow \pi^+ \pi^-$, corresponding to Fig. 1(b),

$$\langle \pi^+(k_+) \pi^-(k_-) | \mathcal{V}^\mu | 0 \rangle_\omega = \frac{e g_{\omega\pi\pi} g_{\omega\gamma} s}{m_\omega^2 - s - im_\omega \Gamma_\omega^{\text{tot}}} (k_+ - k_-)^\mu, \quad (15)$$

where we used $\Sigma \epsilon_\mu^{(\omega)}(q) \epsilon_\nu^{(\omega)}(q) = -g_{\mu\nu} + q^\mu q^\nu / m_\omega^2$. Comparison with Eqs. (6) and (7) allows us to identify

$$\kappa_1 = g_{\omega\pi\pi} g_{\omega\gamma}. \quad (16)$$

Since we have extracted $g_{\omega\gamma}$ above, we may quantify $g_{\omega\pi\pi}$ once κ_1 is fixed from a fit to form factor data. Note that Eq. (14) does not fix the sign of $g_{\omega\gamma}$, which therefore would also leave the sign of $g_{\omega\pi\pi}$ undetermined. However, if ρ -dominance is used to model the isospin-conserving part of the pion form factor and the signs of $g_{\omega\gamma}$ and $g_{\rho\gamma}$ are assumed equal as suggested by $SU(3)$ flavor symmetry, then positive values for κ_1 (that we will find empirically in the following section) show that $g_{\omega\pi\pi}$ has the same sign as a conventional $g_{\rho\pi\pi}$ coupling. Accordingly we assume $g_{\omega\pi\pi}$ to be positive in our analysis. Obviously, the observable $\omega \rightarrow \pi^+ \pi^-$ partial width or branching fraction is independent of this sign.

The expression for the $\eta' \omega \gamma$ vertex, again according to the sign and phase conventions of Refs. [16, 17], is

$$\langle \omega(q) | \mathcal{V}^\mu | \eta'(p) \rangle = g_{\eta' \omega \gamma} \epsilon^{\mu\nu\alpha\beta} p_\nu q_\alpha \epsilon_\beta^{(\omega)}(q). \quad (17)$$

The coupling constant $g_{\eta' \omega \gamma}$ can be determined using

$$\Gamma(\eta' \rightarrow \omega \gamma) = \frac{g_{\eta' \omega \gamma}^2}{32\pi} \left(\frac{m_{\eta'}^2 - m_\omega^2}{m_{\eta'}} \right)^3, \quad (18)$$

and the measured decay width $\Gamma(\eta' \rightarrow \omega \gamma) = (5.17 \pm 0.35) \text{ keV}$ [24], which leads to

$$g_{\eta' \omega \gamma} = -(0.127 \pm 0.004) \text{ GeV}^{-1}, \quad (19)$$

where the negative sign is consistent with the specifications in Refs. [16, 17]. Analogously to the steps followed above, we may combine the vertex given in Eq. (17) with Eq. (9) to find

$$\begin{aligned} \langle \pi^+(k_+) \pi^-(k_-) | \mathcal{V}^\mu | \eta'(p) \rangle \Big|_\omega \\ = \frac{g_{\eta' \omega \gamma} g_{\omega\pi\pi}}{m_\omega^2 - s - i m_\omega \Gamma_\omega^{\text{tot}}} \epsilon^{\mu\nu\alpha\beta} p_\nu q_\alpha (k_+ - k_-)_\beta. \end{aligned} \quad (20)$$

Thus, the comparison with Eqs. (2) and (8) yields

$$\kappa_2 = -2 g_{\omega\pi\pi} g_{\eta' \omega \gamma}. \quad (21)$$

We will see later that κ_2 turns out to be positive empirically, such that Eq. (19) shows consistency with the positive sign for $g_{\omega\pi\pi}$ once more. With these expressions we are prepared to analyze the data for both the pion vector form factor as well as the decay $\eta' \rightarrow \pi^+ \pi^- \gamma$.

It should be clear from the discussions above that $g_{\omega\pi\pi}$ only provides the strength for a pion pair to be produced in the decay of the ω -meson. This pion pair subsequently undergoes final-state interactions that are parametrized via the complex-valued Omnès function $\Omega(s)$, which leads to a significant enhancement of the ω transition rate, since

$|\Omega(m_\omega^2)|^2 \simeq 30$. Accordingly, the partial decay width for the transition $\omega \rightarrow \pi^+ \pi^-$ is given by

$$\Gamma(\omega \rightarrow \pi^+ \pi^-) = \frac{g_{\omega\pi\pi}^2}{48\pi} \frac{(m_\omega^2 - 4m_\pi^2)^{3/2}}{m_\omega^2} |\Omega(m_\omega^2)|^2. \quad (22)$$

We checked numerically that the results change only marginally if we take the finite ω mass distribution into account.

3 Extracting the branching ratio $\omega \rightarrow \pi^+ \pi^-$

3.1 Pion vector form factor

Recent data for the pion vector form factor is available from SND [30], CMD-2 [31], BaBar [32], KLOE [33, 34], labeled below as KLOE10 and KLOE12, respectively, and BESIII [35]. Up to now, only the first of these data sets is included in the averages of the Particle Data Group (PDG) for $\Gamma(\omega \rightarrow \pi^+ \pi^-)$, and none for the pion vector radius. As the fitting ranges we chose all data of the mentioned sets from the lowest-energy point up to $s = 1 \text{ GeV}^2$ —beyond this energy, effects of the excited ρ resonances start to set in that can no longer be parametrized by a polynomial (see e.g. Fig. 1 of Ref. [20]). We use the form factor data provided by the experiments without covariance matrices; these are available only from KLOE (for BESIII there is an uncertainty in the overall normalization factor). We have checked for the KLOE data that the inclusion of the covariance matrices does not change the fit results. For the main results of our study we employ the Omnès function derived from the phase shift based on the best-fit values quoted by the Madrid analysis [6]; as a cross check we also performed fits based on the Bern phase shifts [7].

First we only fit the parameters α_V and κ_1 , keeping the values for the ω mass and width fixed to the central values provided by the PDG [24], namely 782.65 MeV and 8.49 MeV, respectively. The fit parameters as well as the values for χ^2 per degree of freedom are given as Fit 1 in Table 1. We observe that the fits work well in some, but not in all cases: the p -values characterizing the goodness of the fits in particular to the SND and BaBar data are tiny. In addition, not all results are consistent with each other. Of particular interest for this work is the coupling $g_{\omega\pi\pi}$, extracted from each value of κ_1 via Eq. (16). Then using Eq. (22) one can calculate the branching ratio for the transition $\omega \rightarrow \pi^+ \pi^-$ from $g_{\omega\pi\pi}$. This quantity is also shown for all analyses in Table 1 as well as in Fig. 3. We find that most of the results appear consistent, however, the branching ratio extracted from the BaBar analysis is significantly larger than any of the other determinations.

To better understand the reliability as well as uncertainty of the extraction, we performed various additional fits. We

Table 1 Fit results for the pion vector form factor. Fit 1: ω mass and width fixed; Fit 2: ω mass allowed to float; Fits I and II: as Fits 1 and 2, but employing the Omnès function derived from the phase shifts of the Bern analysis [7]. Fits 1- ρ and 2- ρ : as Fits 1 and 2, but fitting the mass parameter m_ρ in the phase shift $\delta_1(s)$ of Ref. [6] as well. Fits 1- ϕ and 2- ϕ : as Fits 1 and 2, but with an Orsay phase. Fixed parameter values are marked by an asterisk (*). The numbers of data points included in the fits are 45 for SND [30], 28 for CMD-2 [31], 268 for BaBar [32], 75 for KLOE10 [33], 60 for KLOE12 [34], and 60 for BESIII [35].

fits	data set	$\alpha_V \times 10$ [GeV ⁻²]	$\kappa_1 \times 10^3$	m_ω [MeV]	ϕ [°]	m_ρ [MeV]	χ^2/dof	$g_{\omega\pi\pi} \times 10^2$	$\mathcal{B}(\omega \rightarrow \pi^+\pi^-)$ [%]	$\langle r_V^2 \rangle$ [fm ²]
Fit 1	SND	0.91(2)	1.73(4)	782.65 *	0 *	773.6 *	3.60	2.96(8)	1.45(8)	0.4377(4)
	CMD-2	0.99(2)	1.60(5)	782.65 *	0 *	773.6 *	1.96	2.73(10)	1.24(9)	0.4395(5)
	BaBar	0.93(1)	2.25(4)	782.65 *	0 *	773.6 *	1.52	3.84(9)	2.45(11)	0.4384(2)
	KLOE10	0.81(1)	1.68(5)	782.65 *	0 *	773.6 *	1.06	2.86(9)	1.35(9)	0.4353(3)
	KLOE12	0.83(1)	1.46(10)	782.65 *	0 *	773.6 *	1.21	2.50(18)	1.03(15)	0.4357(3)
	BESIII	0.91(4)	1.75(13)	782.65 *	0 *	773.6 *	0.82	2.98(23)	1.48(23)	0.4378(9)
Fit 2	SND	0.96(2)	1.80(4)	781.63(10)	0 *	773.6 *	1.21	3.07(8)	1.57(9)	0.4388(4)
	CMD-2	1.04(2)	1.67(6)	782.32(8)	0 *	773.6 *	1.45	2.85(11)	1.35(10)	0.4406(6)
	BaBar	0.93(1)	2.30(4)	781.72(10)	0 *	773.6 *	1.16	3.93(9)	2.58(12)	0.4384(2)
	KLOE10	0.81(1)	1.69(5)	782.87(14)	0 *	773.6 *	1.05	2.88(10)	1.37(9)	0.4353(3)
	KLOE12	0.83(1)	1.45(10)	782.29(43)	0 *	773.6 *	1.21	2.48(18)	1.02(15)	0.4357(3)
	BESIII	0.91(4)	1.78(13)	781.87(45)	0 *	773.6 *	0.78	3.03(23)	1.53(23)	0.4378(9)
Fit I	SND	0.47(2)	1.75(4)	782.65 *	0 *	—	4.15	2.99(8)	1.56(8)	0.4334(4)
	CMD-2	0.53(2)	1.61(5)	782.65 *	0 *	—	1.80	2.75(10)	1.32(9)	0.4348(5)
	BaBar	0.51(1)	2.38(3)	782.65 *	0 *	—	2.74	4.06(9)	2.89(13)	0.4346(2)
	KLOE10	0.36(1)	1.83(5)	782.65 *	0 *	—	1.65	3.11(10)	1.69(11)	0.4308(2)
	KLOE12	0.42(1)	1.68(10)	782.65 *	0 *	—	1.28	2.87(17)	1.44(17)	0.4321(3)
	BESIII	0.50(4)	1.88(13)	782.65 *	0 *	—	0.79	3.21(22)	1.81(25)	0.4342(8)
Fit II	SND	0.52(2)	1.82(4)	781.58(10)	0 *	—	1.41	3.11(8)	1.70(9)	0.4346(4)
	CMD-2	0.59(2)	1.69(5)	782.29(8)	0 *	—	1.13	2.88(10)	1.45(10)	0.4361(6)
	BaBar	0.52(1)	2.44(3)	781.64(9)	0 *	—	2.29	4.17(9)	3.05(13)	0.4347(2)
	KLOE10	0.36(1)	1.84(5)	782.92(13)	0 *	—	1.61	3.14(10)	1.72(11)	0.4308(2)
	KLOE12	0.41(1)	1.68(10)	782.46(33)	0 *	—	1.30	2.86(17)	1.43(17)	0.4321(3)
	BESIII	0.50(4)	1.92(13)	781.80(42)	0 *	—	0.73	3.27(22)	1.88(26)	0.4342(8)
Fit 1- ρ	SND	0.91(2)	1.73(4)	782.65 *	0 *	773.51(27)	3.69	2.95(8)	1.44(8)	0.4379(10)
	CMD-2	0.93(4)	1.63(5)	782.65 *	0 *	774.40(44)	1.92	2.78(10)	1.28(10)	0.4375(15)
	BaBar	0.95(1)	2.09(4)	782.65 *	0 *	772.52(10)	1.12	3.57(9)	2.09(11)	0.4400(4)
	KLOE10	0.80(1)	1.69(5)	782.65 *	0 *	773.75(17)	1.06	2.89(10)	1.39(10)	0.4350(7)
	KLOE12	0.82(2)	1.51(11)	782.65 *	0 *	773.84(27)	1.21	2.57(19)	1.09(17)	0.4352(10)
	BESIII	0.90(4)	1.87(14)	782.65 *	0 *	774.55(41)	0.74	3.19(25)	1.70(26)	0.4366(14)
Fit 2- ρ	SND	0.94(2)	1.81(4)	781.61(10)	0 *	773.96(27)	1.20	3.09(9)	1.60(9)	0.4381(10)
	CMD-2	0.97(4)	1.71(6)	782.30(8)	0 *	774.65(44)	1.29	2.92(11)	1.42(11)	0.4381(15)
	BaBar	0.95(1)	2.15(4)	781.78(10)	0 *	772.61(10)	0.83	3.67(9)	2.23(11)	0.4399(4)
	KLOE10	0.80(1)	1.71(5)	782.87(14)	0 *	773.77(17)	1.04	2.92(10)	1.41(10)	0.4350(7)
	KLOE12	0.82(2)	1.49(11)	782.32(41)	0 *	773.82(27)	1.22	2.54(20)	1.08(17)	0.4352(10)
	BESIII	0.90(4)	1.92(14)	781.80(43)	0 *	774.65(42)	0.68	3.27(25)	1.80(28)	0.4365(14)
Fit 1- ϕ	SND	1.02(2)	1.80(4)	782.65 *	11(1)	773.6 *	1.37	3.07(8)	1.57(9)	0.4404(5)
	CMD-2	1.06(3)	1.69(6)	782.65 *	5(1)	773.6 *	1.38	2.89(11)	1.38(10)	0.4413(6)
	BaBar	0.96(1)	2.31(4)	782.65 *	10(1)	773.6 *	1.07	3.94(9)	2.58(12)	0.4391(2)
	KLOE10	0.81(1)	1.68(5)	782.65 *	-1(2)	773.6 *	1.07	2.86(9)	1.36(9)	0.4353(3)
	KLOE12	0.83(1)	1.46(10)	782.65 *	1(4)	773.6 *	1.23	2.49(18)	1.03(15)	0.4357(3)
	BESIII	0.93(4)	1.77(13)	782.65 *	5(4)	773.6 *	0.81	3.01(23)	1.51(23)	0.4382(9)
Fit 2- ϕ	SND	0.99(2)	1.80(4)	781.99(20)	5(2)	773.6 *	1.13	3.07(8)	1.57(9)	0.4396(5)
	CMD-2	1.06(3)	1.69(6)	782.60(22)	4(3)	773.6 *	1.43	2.89(11)	1.38(11)	0.4412(7)
	BaBar	0.95(1)	2.32(4)	782.27(14)	7(1)	773.6 *	1.05	3.95(9)	2.60(12)	0.4390(2)
	KLOE10	0.81(1)	1.69(5)	782.96(23)	1(3)	773.6 *	1.06	2.89(10)	1.38(9)	0.4354(3)
	KLOE12	0.83(1)	1.45(10)	781.92(72)	-4(6)	773.6 *	1.23	2.47(18)	1.02(15)	0.4356(3)
	BESIII	0.91(4)	1.78(13)	781.65(74)	-3(7)	773.6 *	0.79	3.03(23)	1.53(23)	0.4376(10)

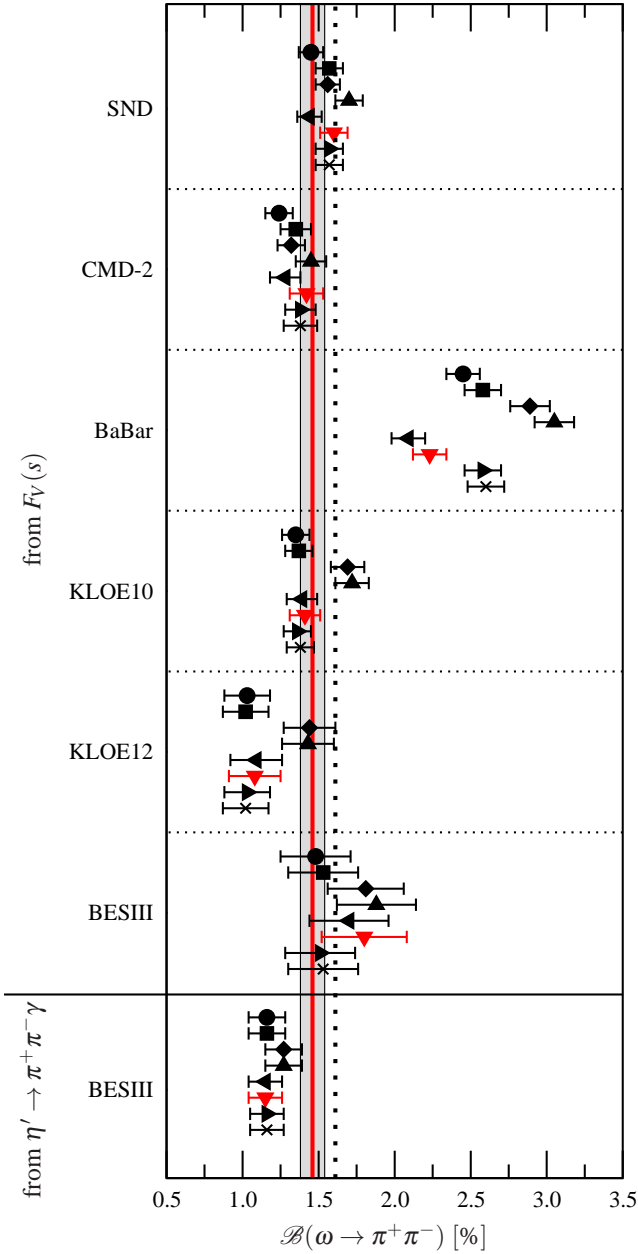


Fig. 3 Comparison of the values for the branching ratio for $\omega \rightarrow \pi^+ \pi^-$ extracted from the various fits to the different data sets, where circles refer to Fit 1, squares to Fit 2, diamonds to Fit I, the triangles-up to Fit II, triangles-left to Fit 1- ρ , (red) triangles-down to Fit 2- ρ , triangles-right to Fit 1- ϕ , and crosses to Fit 2- ϕ . The red thick solid line denotes the average of the values, the gray band the corresponding uncertainty found from our preferred analysis—Fit 2- ρ —omitting the contribution from BaBar. The average with the BaBar value included is shown as the perpendicular dotted line.

account for the possibility of minor shifts in the experimental energy calibration, which may have consequences in particular in view of the narrowness of the ω signal. Hence we repeated the fit described above, allowing the ω mass parameter to float. The corresponding results are

contained in Table 1 as well as in Fig. 3 as Fit 2. We observe that the χ^2/dof improves significantly in particular for the SND and BaBar data, which accordingly are the only two sets for which the fitted ω mass deviates significantly from the PDG value (taking into account both the fit errors as well as the uncertainty quoted by the PDG, $m_\omega = (782.65 \pm 0.12) \text{ MeV}$). We note, however, that the extracted branching ratios $\mathcal{B}(\omega \rightarrow \pi^+ \pi^-)$ are stable throughout within one standard deviation, even in the cases where the overall fit quality improves strongly. We convinced ourselves that replacing the constant ω width by an energy-dependent width as derived, e.g., in Ref. [36] changes the results negligibly.

In addition to the Madrid phase shifts [6] used in most of the fits of our analysis, there is a second high-accuracy analysis of the $\pi\pi$ system available from the Bern group [7]. We thus also performed two fits using these phase shifts: Fit I is based on the ω mass as reported by the PDG, and Fit II allows for a floating ω mass. Overall, the resulting χ^2/dof values tend to be a bit worse compared to the fits based on the Madrid phase shift; in particular, we cannot find acceptable p -values for fits to the BaBar data, not even with a floating ω mass. The extracted $\omega \rightarrow \pi^+ \pi^-$ couplings tend to be somewhat higher than in Fits 1 and 2, see also Fig. 3. Varying the input phase around its central solution within the corresponding uncertainty band in a simplified, linearized manner, we can slightly improve on the fit quality, but not by much; $g_{\omega\pi\pi}$ does not change beyond its error quoted for the various Fits I and II in Table 1. This is most likely not the optimal way to utilize form factor data to fine-tune the Bern phase-shift solution; a more sophisticated attempt to this end is currently under way [37].

In principle, the pion vector form factor provides one of the most precise sources of information on the $\pi\pi$ P -wave interactions, so one could turn the argument around and actually improve the precision of the phase shift $\delta_1(s)$ by adapting it to these data. This has in fact already been done for the Madrid phase shift analysis [8,9], based on older form factor data. Ref. [6] provides an analytic parametrization for $\delta_1(s)$ —cf. Eq. (A7) of this reference—that explicitly contains a mass parameter for the ρ -meson. This parameter denotes the energy at which the phase shift passes through $\pi/2$ (and is therefore not to be confused with the real part of the pole position of the ρ); its allowed range is quoted as $m_\rho = (773.6 \pm 0.9) \text{ MeV}$. In an attempt to optimize the phase shift ourselves in the fit to the pion form factor, we also allowed m_ρ to float. The corresponding fit results appear in Table 1 and Fig. 3 as Fit 1- ρ and Fit 2- ρ for a fixed and a floating ω mass, respectively. Fit 2- ρ finally is flexible enough to yield good fits with reasonable p -values for all six data sets. It is interesting to observe that in all cases but for the fit to the BaBar data, the fits of the ρ -mass parameter

overlap well within uncertainties with the range given by the analysis of Ref. [6].

In the case of the BaBar data we found that the best fit is achieved when both the ρ and the ω mass parameter are shifted downwards by about 1 MeV. This is in contrast to, e.g., the SND data, where the shift in m_ω is also large, however the one in m_ρ is not (and tends to go in the opposite direction). This might suggest that indeed some calibration problem is the origin of the incompatibility of the BaBar results with the remaining data sets; such an explanation has been suggested before [38]. We could show, however, that at least the extracted value for $g_{\omega\pi\pi}$, the main focus of the present study, is still rather insensitive to this (potential) issue: it changed only insignificantly when we re-calibrated the BaBar data by a constant energy shift, adjusted such that the fit returns the central value of the ω mass. Finally, one might wonder whether the larger value of $g_{\omega\pi\pi}$ as extracted from the BaBar analysis is a consequence of the higher energy resolution of that experiment. To test this hypothesis, we combined the BaBar bins in pairs, thus doubling the bin size, and redid the analysis. This again led to an insignificant shift in the extracted value of $g_{\omega\pi\pi}$.

As discussed in Sect. 2.2, the fitting parameters used in our analysis in general, and κ_1 in particular, are necessarily real-valued as a consequence of unitarity. Contrary to this, in many experimental analyses a complex-valued coupling for $\omega \rightarrow \pi^+\pi^-$ is allowed. In order to demonstrate the stability and consistency of our results, we therefore redid Fits 1 and 2, however, now allowing for a complex phase (sometimes called Orsay phase) attached to $g_{\omega\pi\pi}$. The results are reported in both Table 1 as well as Fig. 3 as Fit 1- ϕ and Fit 2- ϕ . One observes that for the three newest data sets (KLOE10, KLOE12, and BESIII) the fits returned phases consistent with zero. However, for the fits to the data by SND, CMD-2, and BaBar in particular, Fit 1- ϕ shows phases that are nonzero by many standard deviations. In contrast, Fit 2- ϕ , where the ω mass parameter was allowed to float, yielded phases for SND and CMD-2 that are only marginally different from 0—the analysis of the BaBar data requires a nonvanishing phase also in this case. The fact that the phases for the SND and CMD-2 fits become consistent with zero once the ω mass is allowed to float is an illustration of the observation that Breit–Wigner parameters are reaction-dependent: a phase in the coupling has a similar effect as a shift in the ω parameters. This is also illustrated in Fig. 4, where we compare real and imaginary parts of two Breit–Wigner functions, namely

$$\begin{aligned} BW_1(s) &= \frac{1}{m_\omega^2 - s - im_\omega\Gamma_\omega^{\text{tot}}}, \\ BW_2(s) &= \frac{e^{i\phi}}{m_\omega^2 - s - im_\omega\Gamma_\omega^{\text{tot}}}, \end{aligned} \quad (23)$$

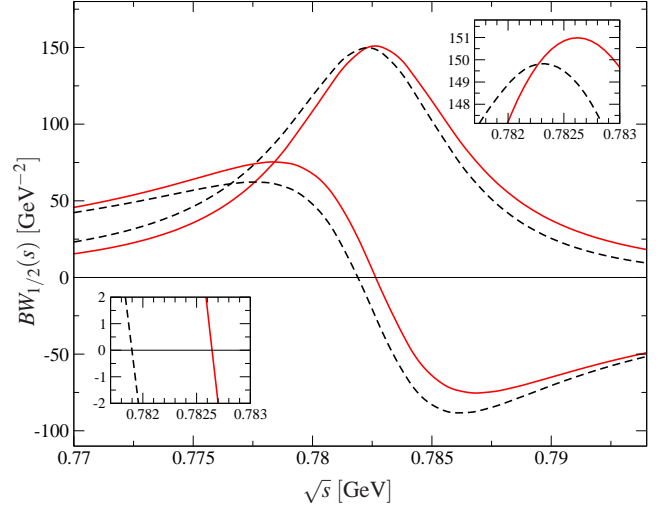


Fig. 4 The line shapes of the amplitudes $BW_1(s)$ and $BW_2(s)$ defined in Eqs. (23) are shown as (red) solid and (black) dashed lines. The peaked lines refer to the imaginary parts, while the ones with a zero refer to the real parts. The inserts magnify the regions of the zero-crossing of the real parts (bottom left) as well as the maximum of the imaginary parts (top right).

using the PDG values for ω mass and width for illustration, as well as $\phi = 10^\circ$. As Fig. 4 demonstrates, introducing this phase in the coupling shifts the peak location of the imaginary part by 0.37 MeV to smaller values of the energy, while the zero in the real part is shifted by 0.75 MeV in the same direction. Note that both shifts are significantly larger than 0.12 MeV, the uncertainty currently quoted for the ω mass by the PDG. The isospin-violating effect that occurs in the pion vector form factor is (dominantly) sensitive to the real part of the Breit–Wigner amplitude, while reactions in which the ω is seen in the 3π channel are largely sensitive to its imaginary part. The fact that the analysis of the BaBar data calls for a nonvanishing phase in the $\omega\pi\pi$ coupling even if the ω mass is allowed to float again points at some inconsistency of those data.

We are now in the position to combine the results from the different experiments. The fits with the least bias are provided by Fit 2- ρ . A weighted average of those results, omitting the result from the BaBar experiment, gives

$$\mathcal{B}(\omega \rightarrow \pi^+\pi^-) = (1.46 \pm 0.08) \times 10^{-2}, \quad (24)$$

where the uncertainty was scaled by a factor 1.5, applying the standard method of the PDG (described in detail in the introduction of the Review of Particle Physics [24]). The result reported in Eq. (24) is consistent with the PDG average of $(1.49 \pm 0.13)\%$ [24], however, with a somewhat reduced uncertainty. We omit the BaBar results from the average on account of the following arguments that seem to indicate an inconsistency within that data set, discussed in detail in this section:

1. the optimal ω mass is outside the range suggested by the PDG;
2. the optimal ρ mass parameter in the $\pi\pi$ P -wave phase parametrization is outside the range determined in Ref. [6];
3. a best fit requires a nonvanishing complex phase of the coupling $g_{\omega\pi\pi}$, which is at odds with unitarity as long as the phase motion of the dominant (isospin-conserving) signal is under control, as it is in our analysis;
4. the BaBar data set is the only one that does not seem to allow for an extraction of the branching fraction $\mathcal{B}(\omega \rightarrow \pi^+\pi^-)$ that is reasonably stable under the different fit variants, see Fig. 3.

If we keep the BaBar data in the average, the branching ratio goes up to $(1.61 \pm 0.15)\%$, with a scaling factor larger than 3. In addition to the theoretical problems, this therefore also points at some inconsistency of the BaBar result with the other experiments.

3.2 $\eta' \rightarrow \pi^+\pi^-\gamma$

While the large number of high-quality data sets on $e^+e^- \rightarrow \pi^+\pi^-$ clearly makes this a preferred reaction to extract $\mathcal{B}(\omega \rightarrow \pi^+\pi^-)$, it appears advisable to access the isospin-violating $\omega \rightarrow \pi^+\pi^-$ decay amplitude also from different reactions. Besides aiming for a further improvement in the statistical precision of the determination of this quantity, we may find further, systematically independent justification for our conclusion on the data selection in the average, namely the omission of the BaBar results. One future option could be the decay $\bar{B}_d^0 \rightarrow J/\psi\pi^+\pi^-$, where the mixing signal shows up very prominently [27]. However, the data presently available in this channel [39] is insufficient for a quantitative analysis.

An alternative is the very recent data on the radiative η' decay $\eta' \rightarrow \pi^+\pi^-\gamma$ from BESIII. We have generated pseudo-data from the preliminary results presented in Ref. [15], where a model-independent fit of a functional form very similar to Eqs. (6) and (8) was used (with, in view of the discussion in the previous subsection, mass and width of the ω fixed to their respective PDG values). BESIII has a data sample of about 9.7×10^5 $\eta' \rightarrow \pi^+\pi^-\gamma$ signal events in 100 energy bins, with very low background (about 1%) and a nearly flat acceptance; therefore, pseudo-data using 9.7×10^5 events should represent the statistical properties of the data set very well. We have performed an analogous series of eight fits as to the form factor data (with fixed and floating m_ω , Madrid and Bern phase input to the Omnès function, fitting m_ρ inside the Madrid phase parametrization, and allowing for an Orsay phase ϕ multiplying the mixing term). The main difference is that the polynomial $P(s)$ has a free normalization constant A

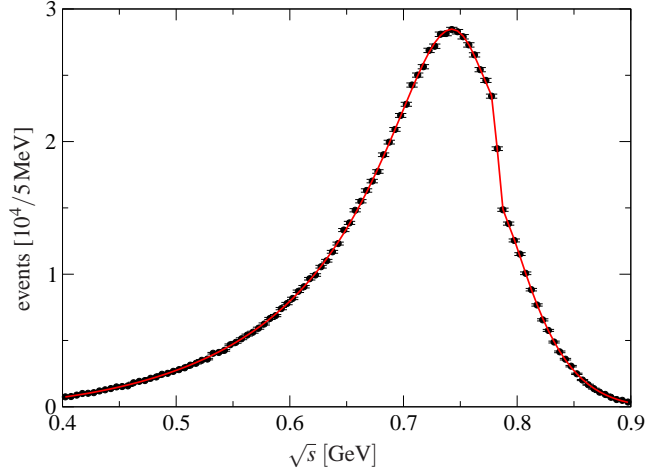


Fig. 5 Best fit to the differential decay rate $d\Gamma(\eta' \rightarrow \pi^+\pi^-\gamma)/d\sqrt{s}$. Pseudo-data generated according to preliminary BESIII results [15].

as well as a curvature term $\propto \beta$, see Eq. (8). All fits were further constrained by the integrated partial width $\Gamma(\eta' \rightarrow \pi^+\pi^-\gamma) = (0.0574 \pm 0.0028) \text{ MeV}$ [24]. Given that we are fitting pseudo-data, it is little surprising that m_ω , m_ρ , and ϕ all come out consistently with their physical values in the cases where they are allowed to float. We mainly include these alternative fits to illustrate the sensitivity of the data to these parameters.

The optimal fit to these pseudo-data is shown in Fig. 5. The resulting fit parameters as well as the corresponding values for the minimal χ^2/dof are displayed in Table 2. They confirm one major finding that was already firmly established for the closely related decay $\eta \rightarrow \pi^+\pi^-\gamma$ [19, 21, 22, 18]: the parameter α is large, about an order of magnitude larger than the corresponding parameter α_V in the form factor fits. Here, however, the BESIII data for the first time demonstrate the necessity of the inclusion of the quadratic term $\propto \beta s^2$ with very high significance. The leading left-hand-cut contribution provided by a_2 -exchange gave an estimate of this parameter, $\beta = (-1.0 \pm 0.1) \text{ GeV}^{-4}$ [18], which yields the correct sign and order of magnitude, but is somewhat larger than what the new data suggest.

In Table 2 we also show the various values of $g_{\omega\pi\pi}$, extracted from κ_2 using Eq. (21), as well as the results for $\mathcal{B}(\omega \rightarrow \pi^+\pi^-)$, which are also added at the bottom of Fig. 3. Here, the variation of coupling constant and branching ratio is entirely negligible over the different fit variants. Although we have only analyzed preliminary pseudo-data at present, the key message is that data of this quality are sufficient to provide an alternative access to the isospin-violating decay $\omega \rightarrow \pi^+\pi^-$ with an accuracy comparable to that of form factor measurements. In addition, the experimental analysis currently available provides a clear preference for smaller values of $\mathcal{B}(\omega \rightarrow \pi^+\pi^-)$, potentially even somewhat below the average cited in Eq. (24), and definitely

Table 2 Fit results for the BESIII [15] pseudo-data of the $\eta' \rightarrow \pi^+\pi^-\gamma$ decay spectrum. Fits 1–II and Fits 1- ρ –2- ϕ are analogous to what is described in Table 1.

fits	A [GeV ⁻³]	α [GeV ⁻²]	β [GeV ⁻⁴]	$\kappa_2 \times 10^3$ [GeV ⁻¹]	m_ω [MeV]	ϕ [°]	m_ρ [MeV]	χ^2/dof	$g_{\omega\pi\pi} \times 10^2$	$\mathcal{B}(\omega \rightarrow \pi^+\pi^-)$ [%]
Fit 1	5.05(13)	0.99(4)	-0.55(4)	6.72(24)	782.65 *	0 *	773.6 *	1.01	2.65(13)	1.16(12)
Fit 2	5.05(13)	1.00(4)	-0.55(4)	6.72(24)	782.78(14)	0 *	773.6 *	1.01	2.65(13)	1.16(12)
Fit I	4.88(13)	1.18(5)	-0.82(5)	6.84(24)	782.65 *	0 *	—	1.32	2.69(13)	1.27(12)
Fit II	4.88(13)	1.18(5)	-0.82(5)	6.84(24)	782.69(14)	0 *	—	1.34	2.69(13)	1.27(12)
Fit 1- ρ	5.08(14)	0.95(7)	-0.50(8)	6.69(24)	782.65 *	0 *	773.39(29)	1.02	2.63(13)	1.15(11)
Fit 2- ρ	5.08(14)	0.95(7)	-0.50(8)	6.68(24)	782.79(15)	0 *	773.36(29)	1.02	2.63(13)	1.15(11)
Fit 1- ϕ	5.05(13)	1.00(4)	-0.56(4)	6.71(24)	782.65 *	-1(1)	773.6 *	1.01	2.64(13)	1.16(11)
Fit 2- ϕ	5.05(13)	0.99(4)	-0.55(4)	6.72(24)	782.79(23)	0(2)	773.6 *	1.02	2.65(13)	1.16(11)

in contradiction to the large numbers found based on the BaBar form factor data.

4 The pion charge radius

On the basis of the present analysis we are now also in the position to extract an improved value for the pion vector radius. It is understood as the square root of the mean squared radius $\langle r_V^2 \rangle$, which in turn is defined by the polynomial expansion of the form factor $F_V(s)$ around $s = 0$,

$$F_V(s) = 1 + \frac{1}{6} \langle r_V^2 \rangle s + \mathcal{O}(s^2). \quad (25)$$

Within the formalism introduced above it may be written as

$$\langle r_V^2 \rangle = \frac{6}{\pi} \int_{4m_\pi^2}^{\infty} dx \frac{\delta_1(x)}{x^2} + 6 \left(\alpha_V + \frac{\kappa_1}{m_\omega^2} \right), \quad (26)$$

where the first term stems from the expansion of the Omnès function, and we have neglected tiny corrections scaling with the ω width in the isospin-breaking contribution (that is very small to begin with). The ratio of two Omnès functions calculated employing two moderately differing high-energy continuations of the phase shifts has a polynomial form at low energies. Since the parameter α_V is determined via a fit to data it therefore implicitly also depends on the high-energy behavior assumed for the phase shifts. However, the pion radius is necessarily independent thereon.²

For the study of the radius we again only use the results of our preferred fit, namely Fit 2- ρ . In order to control the effect of possible correlations between the fitted value of the ρ mass parameter m_ρ and the parameter α_V on the radius, we performed two additional fits to each data set, where we fixed m_ρ to its corresponding minimal and maximal value

²In fact, we have also performed fits with a pion form factor phase (instead of the elastic scattering phase shift) as input to the Omnès function, including effects of the $\rho(1450)$ and $\rho(1700)$ resonances; see Ref. [40] for details. This reduces the parameter α_V almost to zero, however, the radii come out consistent with the present analysis in line with the reasoning given.

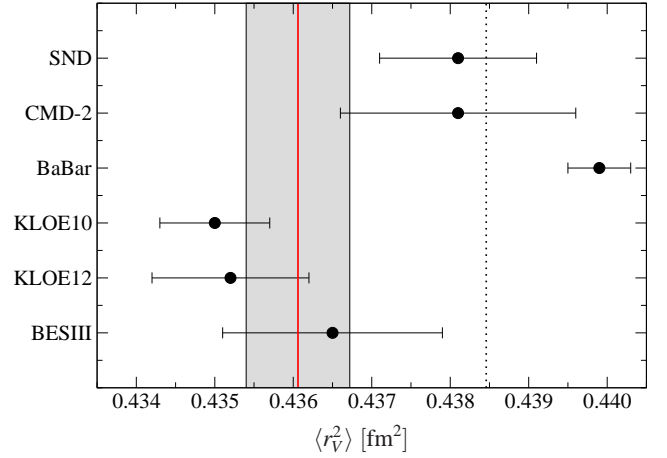


Fig. 6 Comparison of the values for the pion charge radius extracted from the analysis of the different vector form factor data sets. Only the results of our preferred Fit 2- ρ are shown. The red thick solid line denotes the average of the values, the gray band the corresponding uncertainty found omitting the contribution from BaBar. The average with the BaBar value included is shown as the perpendicular dotted line.

allowed by Fit 2- ρ . The uncertainty of the radius is then determined for each experiment from the largest spread in the radii allowed in those fits. The results are shown in Table 1 and Fig. 6.

Averaging the fit results to the individual experiments, omitting again the result from BaBar for the reasons discussed in Sect. 3.1, we find

$$\langle r_V^2 \rangle = (0.4361 \pm 0.0007) \text{ fm}^2, \quad (27)$$

where the uncertainty includes a scale factor of 1.5 determined according to the procedure proposed by the PDG. Our result is consistent with the allowed parameter range for the squared radius between 0.42 fm^2 and 0.44 fm^2 derived on very general grounds in Ref. [41]. This translates into

$$\sqrt{\langle r_V^2 \rangle} = (0.6603 \pm 0.0005) \text{ fm} \quad (28)$$

for the radius, to be compared to the current PDG average $(0.672 \pm 0.008) \text{ fm}$. Both values agree within 2σ ,

however, our number has a significantly reduced uncertainty. It is also interesting to remark that if one keeps only those values in the average quoted in the Review of Particle Physics that were extracted from $e\pi \rightarrow e\pi$ (which basically means omitting values extracted from $eN \rightarrow e\pi N$ that might contain some additional model dependence not included in the uncertainty [42]), the average drops to $(0.663 \pm 0.006) \text{ fm}$, fully in line with the value quoted above, however, with a significantly larger uncertainty. Had we kept the BaBar result, the radius would have shifted to $\langle r_V^2 \rangle = (0.4385 \pm 0.0009) \text{ fm}^2$, which translates to $\langle r_V^2 \rangle^{1/2} = (0.6622 \pm 0.0007) \text{ fm}$, however, here again a scaling factor of 3.3 was necessary for the uncertainty, once more pointing at an inconsistency of the BaBar data compared to the others. This inconsistency is also quite apparent in Fig. 6.

5 Conclusion

Exploiting the universality of final-state interactions by means of dispersion theory as well as the analytic structure of the pion vector form factor and the amplitude for $\eta' \rightarrow \pi^+\pi^-\gamma$, we extracted information on the branching fraction $\mathcal{B}(\omega \rightarrow \pi^+\pi^-)$ and the pion charge radius. Our analysis shows that the BaBar form factor data [32] are inconsistent with the other analyses as well as with theoretical constraints in various respects, but in particular concerning the $\omega \rightarrow \pi^+\pi^-$ coupling strength. It should be noted that other groups came to similar conclusions, see, e.g., Refs. [43, 44]. We therefore do not include the BaBar form factor data in our final averages.

Based on recent data from SND, CMD-2, KLOE, and BESIII, we found $\mathcal{B}(\omega \rightarrow \pi^+\pi^-) = (1.46 \pm 0.08) \times 10^{-2}$ and $\sqrt{\langle r_V^2 \rangle} = (0.6603 \pm 0.0005) \text{ fm}$. Both values are consistent with those currently reported by the PDG [24], however, with reduced uncertainties. Only one of the experiments included in our study has been included in the PDG average for $\mathcal{B}(\omega \rightarrow \pi^+\pi^-)$ so far, and none for the pion charge radius.

We have finally pointed out that high-quality data on $\eta' \rightarrow \pi^+\pi^-\gamma$ will allow one to further improve on the value for $\mathcal{B}(\omega \rightarrow \pi^+\pi^-)$, and cross-check the consistency of the different pion form factor data sets. Final data for this decay can be expected in the very near future from both the CLAS [45] and BESIII [15] collaborations.

Acknowledgements C.W.X. thanks A. Nogga and J. L. Wynen for useful discussions and kind help. Furthermore, we are grateful to G. Colangelo and P. Stoffer for providing us with the pion–pion phase shift solution of Ref. [7]. We thank G. Venanzoni, S. E. Müller, T. Teubner, and A. Keshavarzi for useful communication. This research is supported in part by the DFG and the NSFC through funds provided to the Sino–German CRC 110 “Symmetries and the Emergence of Structure in QCD” (NSFC Grant No. 11621131001, DFG Grant No. TRR110),

and by the National Science Foundation under Grant No. NSF PHY-1125915.

References

1. J. P. Miller, E. de Rafael, B. L. Roberts and D. Stöckinger, *Ann. Rev. Nucl. Part. Sci.* **62**, 237 (2012).
2. T. Blum, A. Denig, I. Logashenko, E. de Rafael, B. Lee Roberts, T. Teubner and G. Venanzoni, arXiv:1311.2198 [hep-ph].
3. M. Benayoun *et al.*, arXiv:1407.4021 [hep-ph].
4. B. Ananthanarayan, G. Colangelo, J. Gasser and H. Leutwyler, *Phys. Rept.* **353**, 207 (2001) [hep-ph/0005297].
5. G. Colangelo, J. Gasser and H. Leutwyler, *Nucl. Phys. B* **603**, 125 (2001) [hep-ph/0103088].
6. R. García-Martín, R. Kamiński, J. R. Peláez, J. Ruiz de Elvira and F. J. Ynduráin, *Phys. Rev. D* **83**, 074004 (2011) [arXiv:1102.2183 [hep-ph]].
7. I. Caprini, G. Colangelo, and H. Leutwyler, *Eur. Phys. J. C* **72**, 1860 (2012) [arXiv:1111.7160 [hep-ph]].
8. J. F. de Trocóniz and F. J. Ynduráin, *Phys. Rev. D* **65**, 093001 (2002) [hep-ph/0106025].
9. J. F. de Trocóniz and F. J. Ynduráin, *Phys. Rev. D* **71**, 073008 (2005) [hep-ph/0402285].
10. H. Leutwyler, hep-ph/0212324.
11. G. Colangelo, *Nucl. Phys. Proc. Suppl.* **131**, 185 (2004) [hep-ph/0312017].
12. B. Ananthanarayan, I. Caprini, D. Das and I. Sentitemsu Imsong, *Phys. Rev. D* **89**, 036007 (2014) [arXiv:1312.5849 [hep-ph]].
13. B. Ananthanarayan, I. Caprini, D. Das and I. Sentitemsu Imsong, *Phys. Rev. D* **93**, 116007 (2016) [arXiv:1605.00202 [hep-ph]].
14. M. Hoferichter, B. Kubis, J. Ruiz de Elvira, H.-W. Hammer and U.-G. Meißner, *Eur. Phys. J. A* **52**, 331 (2016) [arXiv:1609.06722 [hep-ph]].
15. S.-s. Fang [BESIII Collaboration], *PoS CD* **15**, 032 (2016).
16. M. Harada and K. Yamawaki, *Phys. Rept.* **381**, 1 (2003) [hep-ph/0302103].
17. F. Klingl, N. Kaiser and W. Weise, *Z. Phys. A* **356**, 193 (1996) [hep-ph/9607431].
18. B. Kubis and J. Plenert, *Eur. Phys. J. C* **75**, 283 (2015) [arXiv:1504.02588 [hep-ph]].
19. F. Stollenwerk, C. Hanhart, A. Kupść, U.-G. Meißner and A. Wirzba, *Phys. Lett. B* **707**, 184 (2012) [arXiv:1108.2419 [nucl-th]].
20. C. Hanhart, A. Kupść, U.-G. Meißner, F. Stollenwerk and A. Wirzba, *Eur. Phys. J. C* **73**, 2668 (2013); Erratum: [*Eur. Phys. J. C* **75**, 242 (2015)] [arXiv:1307.5654 [hep-ph]].
21. P. Adlarson *et al.* [WASA-at-COSY Collaboration], *Phys. Lett. B* **707**, 243 (2012) [arXiv:1107.5277 [nucl-ex]].
22. D. Babusci *et al.* [KLOE Collaboration], *Phys. Lett. B* **718**, 910 (2013) [arXiv:1209.4611 [hep-ex]].
23. K. M. Watson, *Phys. Rev.* **95**, 228 (1954).
24. C. Patrignani *et al.* [Particle Data Group Collaboration], *Chin. Phys. C* **40**, 100001 (2016).
25. S. Gardner and H. B. O’Connell, *Phys. Rev. D* **57**, 2716 (1998); Erratum: [*Phys. Rev. D* **62**, 019903 (2000)] [hep-ph/9707385].
26. C. Hanhart, *Phys. Lett. B* **715**, 170 (2012) [arXiv:1203.6839 [hep-ph]].
27. J. T. Daub, C. Hanhart and B. Kubis, *JHEP* **1602**, 009 (2016) [arXiv:1508.06841 [hep-ph]].
28. U.-G. Meißner, *Phys. Rept.* **161**, 213 (1988).
29. H. B. O’Connell, B. C. Pearce, A. W. Thomas and A. G. Williams, *Phys. Lett. B* **354**, 14 (1995) [hep-ph/9503332].
30. M. N. Achasov *et al.*, *J. Exp. Theor. Phys.* **103**, 380 (2006) [*Zh. Eksp. Teor. Fiz.* **130**, 437 (2006)] [hep-ex/0605013].

-
31. R. R. Akhmetshin *et al.* [CMD-2 Collaboration], Phys. Lett. B **648**, 28 (2007) [hep-ex/0610021].
 32. B. Aubert *et al.* [BaBar Collaboration], Phys. Rev. Lett. **103**, 231801 (2009) [arXiv:0908.3589 [hep-ex]].
 33. F. Ambrosino *et al.* [KLOE Collaboration], Phys. Lett. B **700**, 102 (2011) [arXiv:1006.5313 [hep-ex]].
 34. D. Babusci *et al.* [KLOE Collaboration], Phys. Lett. B **720**, 336 (2013) [arXiv:1212.4524 [hep-ex]].
 35. M. Ablikim *et al.* [BESIII Collaboration], Phys. Lett. B **753**, 629 (2016) [arXiv:1507.08188 [hep-ex]].
 36. M. Hoferichter, B. Kubis, S. Leupold, F. Niecknig and S. P. Schneider, Eur. Phys. J. C **74**, 3180 (2014) [arXiv:1410.4691 [hep-ph]].
 37. P. Stoffer, private communication.
 38. M. Benayoun, P. David, L. DelBuono and F. Jegerlehner, Eur. Phys. J. C **75**, 613 (2015) [arXiv:1507.02943 [hep-ph]].
 39. R. Aaij *et al.* [LHCb Collaboration], Phys. Rev. D **90**, 012003 (2014) [arXiv:1404.5673 [hep-ex]].
 40. S. P. Schneider, B. Kubis and F. Niecknig, Phys. Rev. D **86**, 054013 (2012) [arXiv:1206.3098 [hep-ph]].
 41. B. Ananthanarayan, I. Caprini, D. Das and I. Sentitemsu Imsong, Eur. Phys. J. C **73**, 2520 (2013) [arXiv:1302.6373 [hep-ph]].
 42. A. Liesenfeld *et al.* [A1 Collaboration], Phys. Lett. B **468**, 20 (1999) [nucl-ex/9911003].
 43. B. Ananthanarayan, I. Caprini, D. Das and I. Sentitemsu Imsong, Eur. Phys. J. C **72**, 2192 (2012) [arXiv:1209.0379 [hep-ph]].
 44. M. Benayoun, P. David, L. DelBuono and F. Jegerlehner, Eur. Phys. J. C **73**, 2453 (2013) [arXiv:1210.7184 [hep-ph]].
 45. M. C. Kunkel [CLAS Collaboration], AIP Conf. Proc. **1735**, 030017 (2016).